Electronic supplementary information

From egg-shell to uniform distribution of platinum by atomic layer deposition on mesoporous alumina spheres: Experiments and modeling

Christine Gonsalves,*[a], Jänis Järvilehto,[a,b] Saeed Saedy,[b] Jorge A. Velasco,[a] Thomas Grehl,[c] Philipp Brüner,[c] Niko Heikkinen,[d] Juha Lehtonen,[d] J. Ruud van Ommen,[b] and Riikka L. Puurunen*[a]

Contents

[a] *Department of Chemical and Metallurgical Engineering, Aalto University, P.O. Box 16100, FI-00076 AALTO, Finland.*
[b] *Department of Chemical Engineering, Process and Product Technology Institute, Delft University of Technology, Van der Maasweg 9, 2629 HZ Delft, The Netherlands.*
[c] *IONTOF GmbH, Münster, Germany*
[d] *VTT Technical Research Center Finland, P.O. Box 1000, FI-02044 VTT, Finland.*
† Electronic supplementary information (ESI) available.
* Corresponding authors. E-mail:christine.gonsalves@aalto.fi, riikka.puurunen@aalto.fi

S1 Experimental details

S1.1 Model description

In this work, we use a diffusion–reaction model[1] for ALD on porous spheres to compare the radial evolution of surface coverage with experimental results. The effective diffusion coefficient D_{eff} (m^2s^{-1}) valid for any diffusion regime is calculated as[1,2] (also equation 4 in the main manuscript):

$$D_{\text{eff}} = \frac{\varepsilon}{\tau} \cdot \left(\frac{1}{\frac{1}{D_{\text{A}}} + \frac{1}{D_{\text{Kn}}}} \right). \tag{1}$$

Here, ε is porosity (-), τ is tortuosity (-), D_{A} ($\text{m}^2\,\text{s}^{-1}$) is the molecular diffusion coefficient of the reactant gas and D_{Kn} ($\text{m}^2\,\text{s}^{-1}$) is the Knudsen diffusion coefficient.

The molecular diffusion coefficient D_{A} accounts for the thermal velocity and collision frequency of the reactant (gas A) and inert gases (gas I). It is expressed by[3,4]:

$$D_{\text{A}} = \frac{3\pi \overline{v}_{\text{A}}{}^2}{16 z_{\text{A}}}, \tag{2}$$

where $\overline{v}_{\text{A}}$ is thermal velocity *i.e.,* the average speed ($\text{m}\,\text{s}^{-1}$)[3,4], given by

$$\overline{v}_{\text{A}} = \sqrt{\frac{8RT}{\pi M_{\text{A}}}}. \tag{3}$$

The z_{A} is the collision frequency is calculated from[3,4]

$$z_{\text{A}} = \frac{\pi}{4}(d_{\text{A}} + d_{\text{I}})^2 \sqrt{\frac{8RT}{\pi}\left(\frac{1}{M_{\text{A}}} + \frac{1}{M_{\text{I}}}\right)} \frac{p_{\text{I}} N_0}{RT} + \pi (d_{\text{A}})^2\, 4 \sqrt{\frac{RT}{\pi M_{\text{A}}}} \frac{p_{\text{A}} N_0}{RT}. \tag{4}$$

Here, d_{A} and d_{I} (m) are the hard-sphere diameters of reactant and inert gas, M_{A} and M_{I} ($\text{kg}\,\text{mol}^{-1}$) are the molecular weights of the reactant and inert gas, N_0 is Avogadro's constant (mol^{-1}) and p_{I}

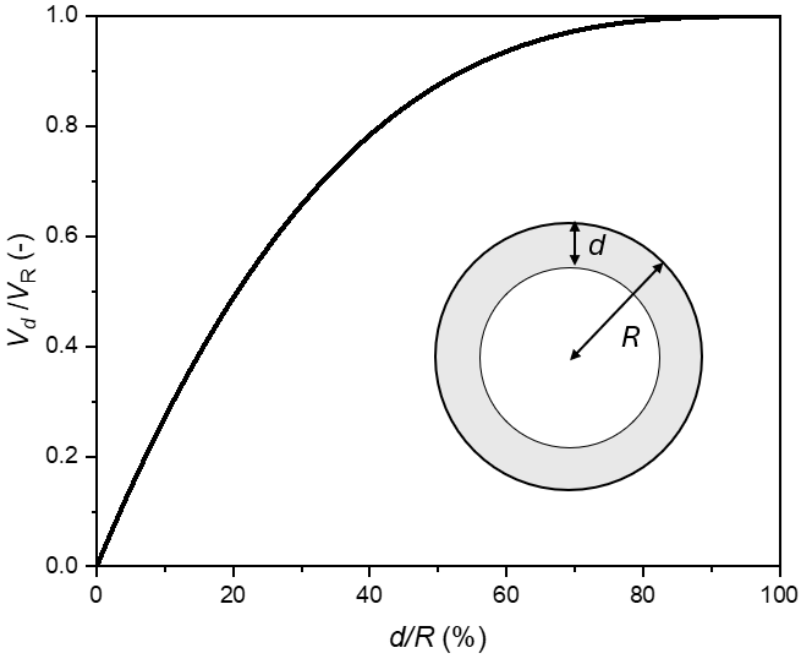

Figure S1 Ratio of coated volume to total internal volume as a function of percentage penetration depth within a spherical porous particle. This figure was recreated from Refs.[6] and[7].

(Pa) is the partial pressure of the inert gas. The Knudsen diffusion coefficient[1,4,5] is given by

$$D_{\mathrm{Kn}} = d_{\mathrm{pore}} \sqrt{\frac{8RT}{9\pi M_{\mathrm{A}}}}. \tag{5}$$

Here, d_{pore} is the pore diameter (m), R (8.314 $\mathrm{JK^{-1}mol^{-1}}$) is the universal gas constant, T (K) is the temperature of the ALD process, and M_{A} ($\mathrm{kg\,mol^{-1}}$) is the molar mass of the reactant gas.

S1.2 Kn number and Thiele modulus calculation

The Knudsen number Kn (dimensionless) is a ratio of the mean free path λ (m) of a gas molecule to a characteristic physical length scale, in this case the pore diameter d_{pore} (m) given by[3–5]

$$\mathrm{Kn} = \frac{\lambda}{d_{\mathrm{pore}}}. \tag{6}$$

For a system of two gases, the mean free path is calculated as[3–5]

$$\lambda = \frac{k_{\mathrm{B}} T}{\sqrt{2} p_{\mathrm{A0}} \sigma_{\mathrm{A,A}} + \sqrt{1 + \frac{m_{\mathrm{A}}}{m_{\mathrm{I}}}} p_{\mathrm{I}} \sigma_{\mathrm{A,I}}}, \tag{7}$$

where k_{B} (J K^{-1}) is the Boltzmann constant, T (K) is the temperature, and m_{A} and m_{I} (kg) are the masses of the molecules of reactant A and inert gas I, respectively. Also, p_{A_0} (Pa) is the partial pressure of reactant A and p_I (Pa) is the inert gas partial pressure. The $\sigma_{A,A}$ and $\sigma_{A,I}$ are the collision cross sections (m^2) between the molecules i and j, given by[3–5]

$$\sigma_{\mathrm{i,j}} = \pi \left(\frac{d_{\mathrm{i}}}{2} + \frac{d_{\mathrm{j}}}{2} \right)^2, \tag{8}$$

where d_i (m) and d_j (m) are the hard-sphere diameters of the molecules i and j, respectively.

The Thiele modulus h_{T} (-) is calculated from[5,8]:

$$h_{\mathrm{T}} = R \sqrt{\frac{c\ \bar{v}_{\mathrm{A}}}{2\ d_{\mathrm{pore}}\ D_{\mathrm{eff}}}}, \tag{9}$$

where R (m) is the sphere radius.

S1.3 CO pulse chemisorption calculations

From the cumulative amount of CO gas chemisorbed (results in Table 4 of the main manuscript), the metal dispersion (D) and hemispherical crystallite size were calculated as described below.

Dispersion D is the fraction of metal atoms that are accessible on the surface (N_{s}) relative to the total number of metal atoms in the sample (N_{tot}):

$$D = \frac{N_{\mathrm{s}}}{N_{\mathrm{tot}}}.$$

The dispersion is calculated from the quantity of CO chemisorbed as follows:

$$D = \frac{V_{\mathrm{ads,irr}} \times n \times M_{\mathrm{M}}}{V_{\mathrm{mol}} \times w_{\mathrm{M}}},$$

where $V_{\mathrm{ads,irr}}$ is the volume of irreversibly chemisorbed CO at STP (cm^3 g^{-1}), n is the stoichiometric

factor (number of CO molecules adsorbed per surface metal atom, here $n = 1$), M_M is the atomic weight of the metal ($g\,mol^{-1}$), V_{mol} is the molar volume of the adsorbate gas at STP (22.414 L/mol equal to 22 414 $cm^3\,mol^{-1}$), and w_M (wt%) is the metal weight loading of the sample.

The surface area of the active metal per gram of sample, A_M ($m^2\,g^{-1}_{sample}$), can be calculated from the amount of irreversibly adsorbed CO using

$$A_M = \frac{V_{ads,irr} \times N_0 \times n \times a_M}{V_{mol}},$$

where a_M is the average surface area of a single metal atom (in this case Pt atomic cross sectional area is 0.080 nm^2 and the density of Pt is 21.45 $g\,cm^{-3}$)[9,10].

Once the metal surface area and total metal content are known, the average particle size can be estimated using geometrical assumptions, assuming hemispherical particles. For a sphere, the volume-to-surface area ratio is $V_R/A_R = R/3$, where V_R is the total internal volume of a sphere of radius R, and A_R is the surface area of the sphere. Knowing the metal loading w_M (wt%) and the bulk metal density ρ_M ($g\,cm^{-3}$), the particle radius can be calculated as $R_M = 3w_M/(\rho_M A_M)$, where A_M is the measured metal surface area. The corresponding average particle diameter is twice the radius, $d_M = 2R_M = 6w_M/(\rho_M A_M)$.

S1.4 Selection of the fluidization conditions

Tests were done to estimate the fluidization velocity for the alumina spheres. For the tests, a mixture of 25 g of glass beads (diameter: 125-150 μm) and several porous alumina spheres (diameter: 2.5 mm, SASOL Limited) was fluidized at room temperature at superficial gas velocities ranging from 1.7 cm/s (0.5 l/min) to 3.4 cm/s (1 l/min), [normal liter per second, at 1 atm and 20 °C] to determine the minimum fluidization velocity, U_{mf}. The alumina spheres (originally white in color) were treated with ink to ease the assessment of particle circulation in the bed. The fluidization tests indicated a minimum fluidization velocity, U_{mf} of approximately 2.7 cm/s, achieved with a flow rate of 0.80 l/min through the column. Thus, a flow rate of 1.0 l/min was selected for the experiments, resulting in a fluidization velocity of approximately 3.4 cm/s.

S1.5 Fluidized bed reactor schematic

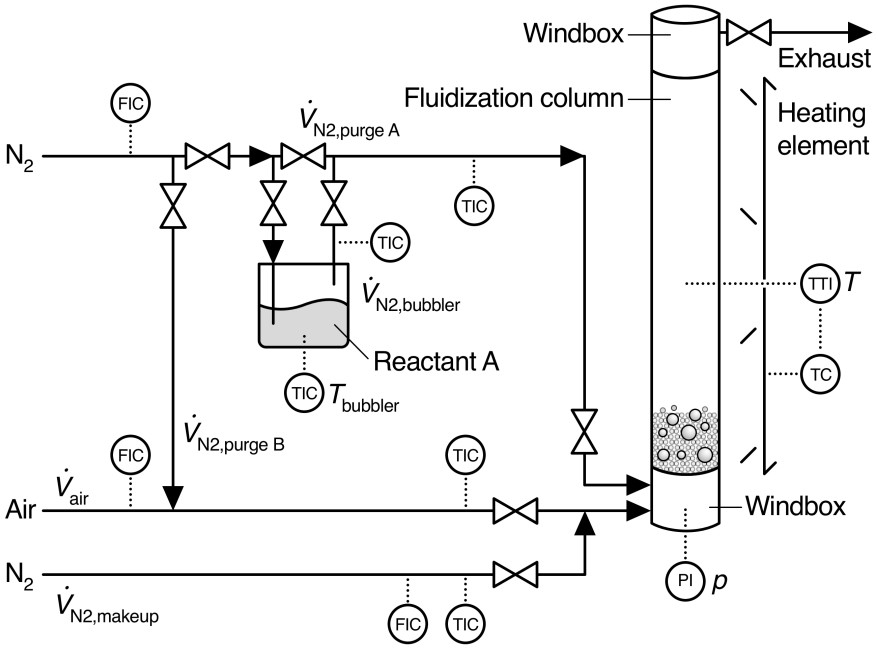

Figure S2 Simplified schematic of the ALD equipment[11]. The instrumentation used to monitor and control the process includes control valves, flow indicators and controllers (FIC), temperature indicators and controllers (TIC), a temperature transmitter and indicator (TTI), a temperature controller (TC) and a pressure indicator (PI). In the fluidization column, glass beads are denoted by small, faint circles, while the large, shaded circles represent porous alumina spheres. This reactor was similar to that used in the Grillo et al. work[12].

S2 Results

S2.1 Support Characterization

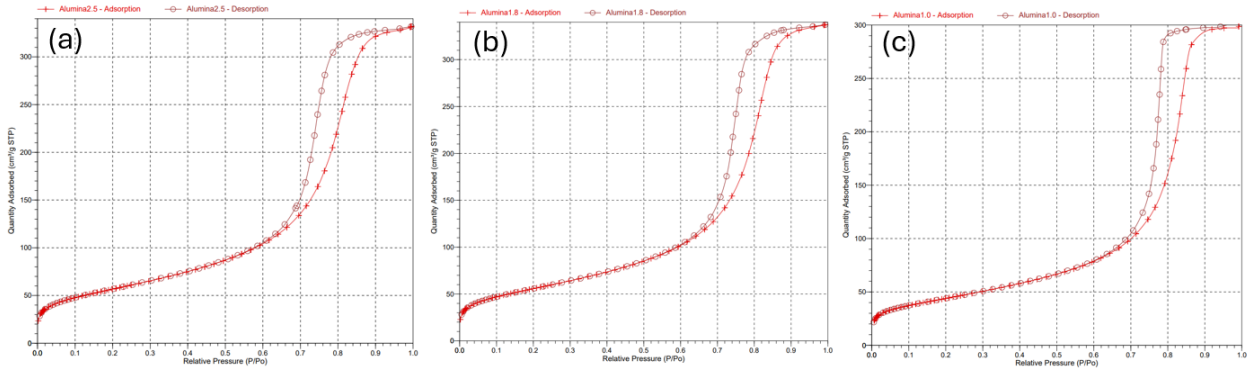

Figure S3 Nitrogen adsorption-desorption isotherm of the alumina spheres of varying diameters: (a) 2.5 mm, (b) 1.8 mm, and (c) 1.0 mm. The plot exhibits a Type IV(a) isotherm with a hysteresis loop, characteristic of mesoporous materials.

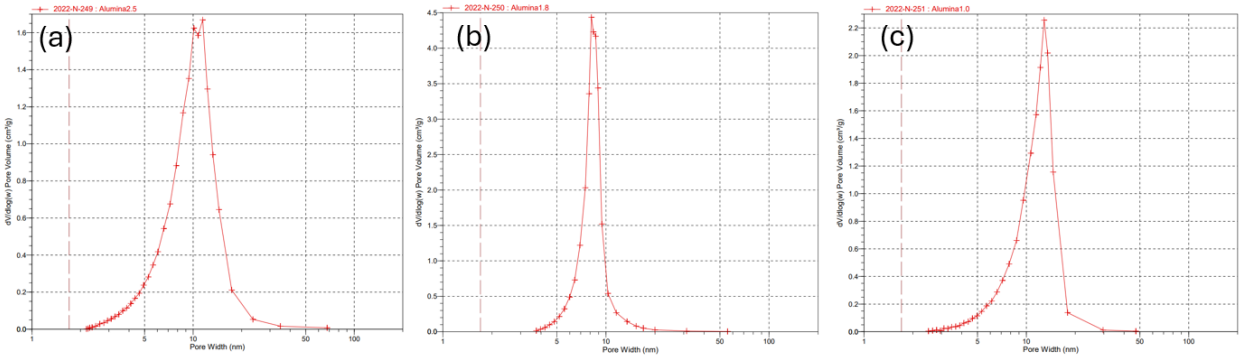

Figure S4 Barrett-Joyner-Halenda (BJH) pore size distributions for alumina spheres of varying diameters: (a) 2.5 mm, (b) 1.8 mm, and (c) 1.0 mm. All samples show a narrow pore size distribution in the mesoporous range.

S2.2 Average areal number density calculation example

The average areal number density $c_{\mathrm{M}}(\mathrm{nm}^{-2})$ can be calculated[13,14] using Equation 1 of the main manuscript, also written here:

$$c_{\mathrm{M}} = \frac{w_{\mathrm{M}} N_0}{M_{\mathrm{M}} S} \frac{m_{\mathrm{t}}}{m_{\mathrm{s}}}. \tag{10}$$

Here, w_{M} is the weight fraction of the metal, N_0 (mol^{-1}) is Avogadro's constant, M_{M} ($\mathrm{g_{metal}\,mol^{-1}}$) is the molar mass of the metal, S ($\mathrm{m^2\,g^{-1}_{support}}$) is the specific surface area of the support, m_{t} ($\mathrm{g_{sample}}$) is the total mass of the sample including the amount of the deposited material, and m_{s} ($\mathrm{g_{support}}$) is the mass of the original support.

Now since $m_{\mathrm{t}} = m_{\mathrm{s}} + m_{\mathrm{Pt}}$, and $w_M = m_{\mathrm{Pt}}/m_t$; $\mathrm{m_{Pt}}$ being the mass of the deposited Pt,

$$\frac{m_t}{m_s} = \frac{m_t}{m_t - m_{Pt}} = \frac{m_t}{m_t - (w_M \cdot m_t)} = \frac{1}{1 - w_M}$$

Equation 10 thus becomes:

$$c_{\mathrm{M}} = \frac{w_{\mathrm{M}} N_{\mathrm{A}}}{M_{\mathrm{M}} S} \frac{1}{1 - w_M}. \tag{11}$$

In this work, the Pt loading in terms of wt% after five cycles, with an exposure time of 1440 s for the 2.5 mm sphere, was 4.00 wt% The specific surface area S of the alumina support was 206 $\mathrm{m^2\,g^{-1}}$, Avogadro's constant is 6.022×10^{23} $\mathrm{mol^{-1}}$, and the molar mass of Pt is 195 $\mathrm{g\,mol^{-1}}$. Plugging these values into the above equation:

$$c_{\mathrm{M}} = \frac{\left(\frac{5.61}{100}\right) \times 6.022 \times 10^{23}\,\mathrm{mol^{-1}}}{195\,\mathrm{g\,mol^{-1}} \times 206\,\mathrm{m^2 g^{-1}}} \frac{1}{1 - \left(\frac{5.61}{100}\right)}$$

$$c_{\mathrm{M}} = 0.62 \text{ Pt atoms/nm}^2$$

The average areal number density c_{M} after five ALD cycles is 0.62 Pt atoms/$\mathrm{nm^2}$, so after one cycle, the average areal number density is 0.12 $\mathrm{nm^{-2}}$. This calculation assumes that the mass of Pt added to the sample after ALD does not affect the total surface area of the sample.

S2.3 Metal weight loading: ICP-OES results

Table S1 Numerical values for average Pt loading (wt%) for the different sphere diameters from ICP-OES results of Figure 1a of the main manuscript. Calculated values for the average areal number density (Figure 1b of the main manuscript) are also shown.

Exposure time (s)	Pt loading (wt%)			Average areal number density, Five cycles (Pt atoms/nm^2)			Average areal number density, One cycle, (Pt atoms/nm^2)		
	1.0 mm	1.8 mm	2.5 mm	1.0 mm	1.8 mm	2.5 mm	1.0 mm	1.8 mm	2.5 mm
180	1.38	1.26	0.94	0.27	0.20	0.14	0.05	0.04	0.03
360	1.76	2.06	1.64	0.35	0.32	0.25	0.07	0.06	0.05
720	2.47	3.07	2.85	0.49	0.48	0.44	0.10	0.10	0.09
1440	3.51	4.05	4.00	0.71	0.65	0.62	0.14	0.13	0.12

For the largest sphere size with a diameter of 2.5 mm (radius R = 1.25 mm), for which the coating penetration profile was measured (Figure 3 of the main article) it was possible to estimate the penetration depth d, and the areal number density of Pt in the specific coated area of the sphere A_{coat}, the results are shown in Table S2. This areal number density is not an average value but is based on the coated volume fraction ϕ_{coat} discussed in Equation 8 of the main article, also written here below as:

$$\phi_{\text{coat}} = \frac{V_{\text{d}}}{V_{\text{R}}} = \frac{\left(R^3 - (R-d)^3\right)}{R^3}. \tag{12}$$

The reported values of the areal number density (Table S2) are estimates based on the visual determination of the penetration depth d at half coverage, from the LEIS results (Figure 3 of the main article), and the coated volume fraction ϕ_{coat} (Equation 12). The calculation assumes a step-like saturation profile, which is a simplification compared to the more gradual saturation fronts observed experimentally.

The specific coated area of the sphere A_{coat} was determined from:

$$A_{\text{coat}} = S \times \phi_{\text{coat}}. \tag{13}$$

The areal number density based on the coated volume fraction was calculated using the relation:

$$c_{\text{M}} = \frac{w_{\text{M}} N_0}{M_{\text{M}} A_{\text{coat}}} \frac{m_{\text{t}}}{m_{\text{s}}}, \tag{14}$$

and is reported in Table S2. The areal number density calculated in this way (i.e., based on the coated volume fraction) increases slowly with increasing exposure time.

Table S2 Areal number density for the sphere of diameter 2.5 mm (Specific surface area $S = 206$ m^2/g) based on the coated volume fraction of the sphere.

Exposure time t (s)	Pt loading (wt%)	Penetration depth d^a (μm)	Coated volume fraction ϕ_{coat} (-)	Areal number density based on ϕ_{coat} (Pt atoms/nm^2)	Areal number density based on ϕ_{coat}, One cycle (Pt atoms/nm^2)
180	0.94	300	0.561	0.25	0.05
360	1.64	500	0.784	0.32	0.06
720	2.85	1150	0.999	0.44	0.09
1440	4.00	1250	1.000	0.62	0.12

[a] Penetration depth was estimated from the LEIS results (Figure 3 of the main article), as the distance where the Pt intensity reduced to half of its initial value.

S2.4 Pulse Chemisorption results: Characterization with mass spectroscopy

Table S3 Characterization results from CO pulse chemisorption (mass spectrometry measurements, m/z=28 (CO)) done on Pt-coated alumina spheres of diameter 2.5 mm.

$MeCpPtMe_3$ exposure time (s)	Cumulative CO quantity (cm^3) (STP)	Cumulative CO quantity (μ mol/g)	Cumulative quantity (CO (molecules) /nm^2)	ICP-OES weight loading (%) for 2.5 mm sphere)	Areal number density (Pt atoms /nm^2)	Crystallite size (hemisphere) (nm)	Metal dispersion
180	1.31	58.26	0.17	0.94	0.14	-[a]	-[a]
360	-[b]	-[b]	-[b]	1.64	0.25	-[b]	-[b]
720	2.69	119.85	0.35	2.85	0.44	1.38	82.04%
1440	2.55	113.95	0.33	4.00	0.62	2.04	55.58 %

[a] The cumulative quantity of CO chemisorbed in terms of the CO molecules/nm^2 of the surface exceeded the corresponding number of Pt atoms/nm^2. The stoichiometry in this case may differ from the stoichiometry value of one used in the dispersion and crystallite size calculations.

[b] During the CO pulse chemisorption measurements, there was an instrumental failure in the mass spectrometer during the experiment and hence data was not collected.

S2.5 Low-energy ion scattering

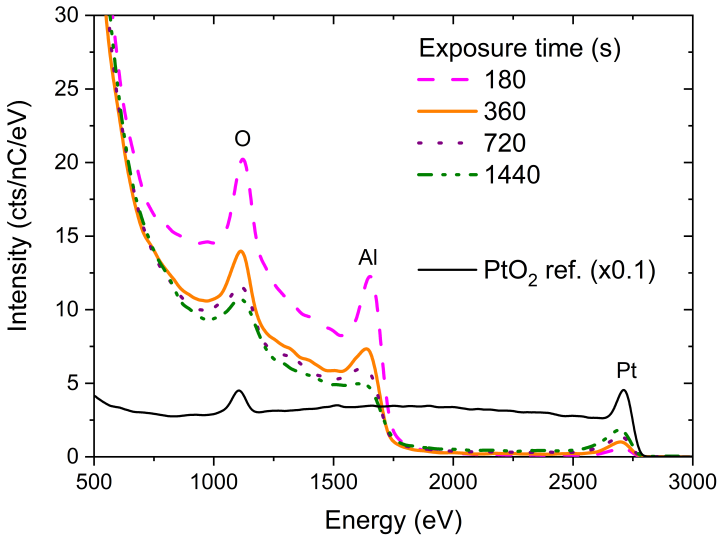

Figure S5 Representative example LEIS spectra (averaged over the entire cross-sectional area of the sphere) corresponding to Figures 2 and 3 of the main article. A PtO_2 powder reference (Sigma-Aldrich, CAS 1314-15-4) is included and plotted scaled ×0.1. O, Al, and Pt peaks are labeled.

S2.6 X-ray photoelectron spectroscopy

The atomic fraction of platinum within the porous alumina spheres were determined by Thermo Scientific K Alpha X-ray photoelectron spectroscope (XPS). Before analysis, the spheres were mechanically cut approximately in half with scissors to obtain cross-sections. In each scan, an elliptical area of $\sim$ 380 μm x 770 μm was scanned with a monochromated X-ray, emitted from aluminum Kα radiation. A photon energy of 1486.7 eV was used with a step size of 0.157 eV. A flood gun was employed to compensate for the differential charging. The peak locations were calibrated using the aliphatic carbon 1s peak (located at 284.8 eV). The CasaXPS software was used to interpret the acquired spectra.

Figure S6 presents XPS line scans showing Pt distribution from the outer surface to the center and back, of porous spheres of size 2.5 mm after ALD with different exposure times. With an increase in exposure time, the overall value of the Pt signal, including its initial value, increased. For exposure times of 180, 360, and 720 s, the atomic fraction of Pt decreased along the porous sphere, reached a plateau at its center, and then increased again toward the outer surface of the porous sphere. For the sample with the longest exposure time of 1440 s, a minor decrease in the metal fraction was observed at the center (change was about 5% of the original value from 1.52 % to 1.44%), whereas the overall distribution of Pt was seen to be uniform across the porous sphere. The increasing XPS signal intensity at the outer edges of the particle with time is consistent with the increasing platinum areal number density calculated for the coated volume fraction by combining the LEIS results and weight loading data from ICP-OES (Table S2).

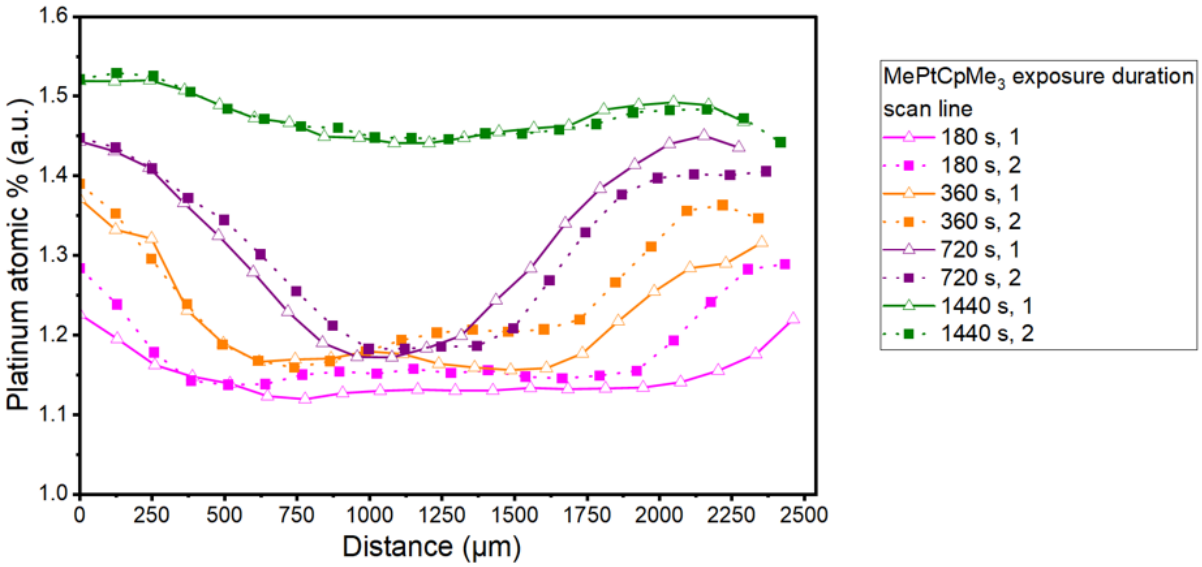

Figure S6 Atomic percentage of platinum along the radial direction from XPS analysis on a cross-section of 2.5 mm diameter alumina spheres for different exposure times. Two scans per particle along the radius were done (see Figure S7 for scan directions).

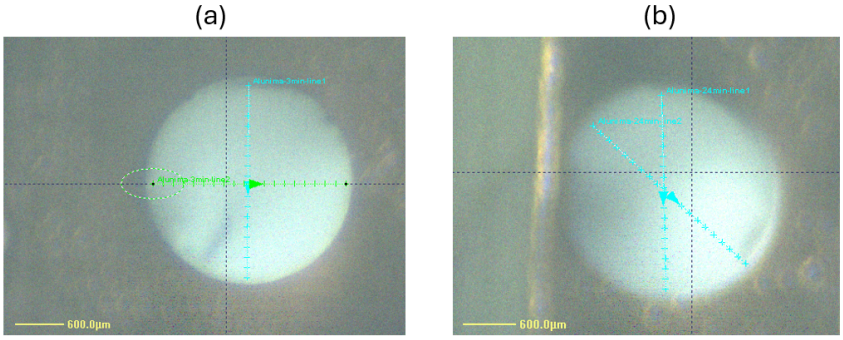

Figure S7 Siting of XPS scans from images taken from the optical camera of the XPS instrument on the cross-sections of the cleaved 2.5 mm alumina spheres. Samples with exposure times of 180, 360, and 720 s were scanned as shown in Panel (a), and the sample with exposure time of 1440 s was scanned as in Panel (b). The direction of the scans were selected to avoid rough surfaces with large voids or terraces as a result of sample cleavage.

S2.7 Diffusion–reaction modeling

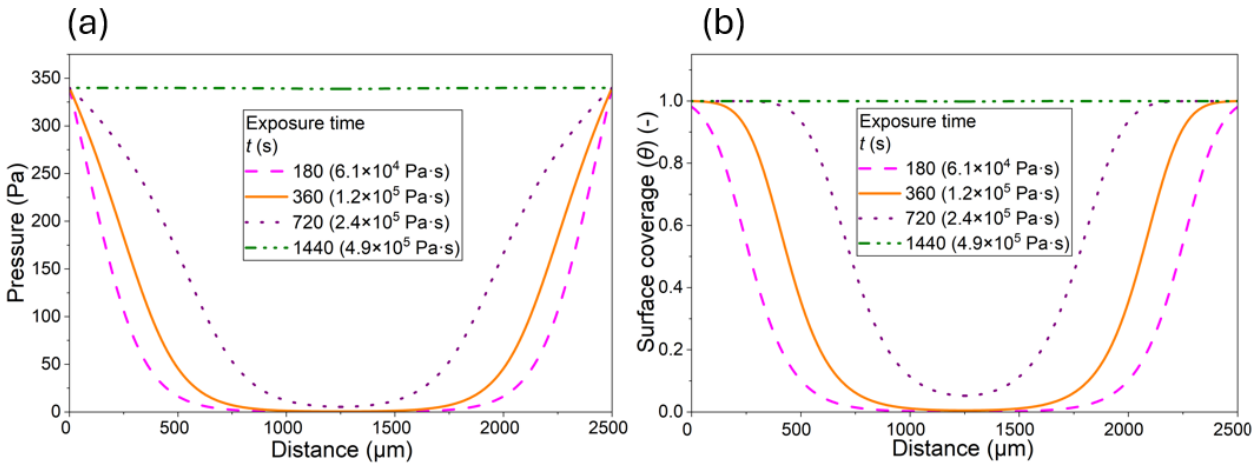

Figure S8 $MePtCpMe_3$ pressure profiles corresponding to the saturation profiles shown in panel (b). Panel (b) saturation profiles are the same as in Figure 4a of the main article.

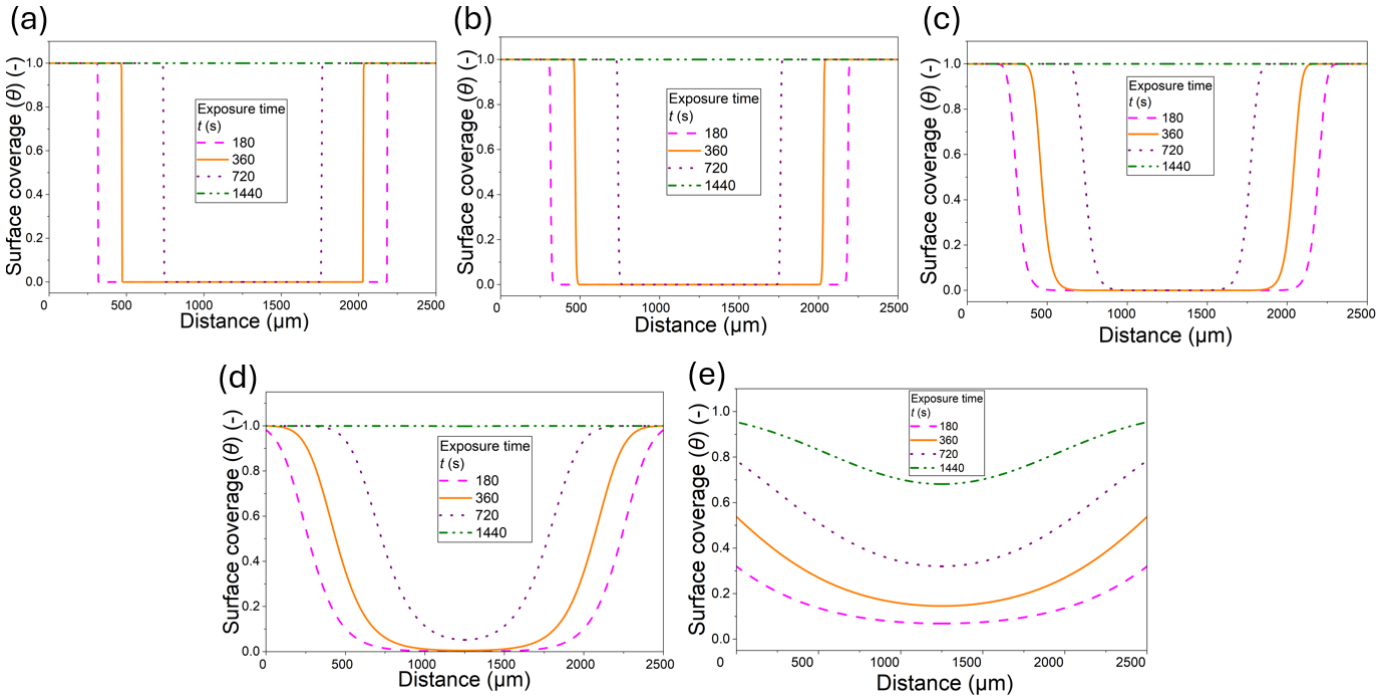

Figure S9 Simulated surface coverage profiles, along the radial direction from the outer surface towards the center and back, along the radius of a 2.5 mm alumina sphere for different sticking coefficients: (a) $c = 10^{-3}$, (b) $c = 10^{-6}$, (c) $c = 10^{-8}$, (d) $c = 10^{-9}$, and (e) $c = 10^{-10}$. Other simulation parameters are as specified in the caption of Figure 4 of the main article.

References

[1] N. Heikkinen, J. Lehtonen and R. L. Puurunen, An atomic layer deposition diffusion–reaction model for porous media with different particle geometries, *Physical Chemistry Chemical Physics*, 2024, **26**, 7580–7591.

[2] R. Evans III, G. Watson and E. Mason, Gaseous diffusion in porous media at uniform pressure, *The journal of chemical physics*, 1961, **35**, 2076–2083.

[3] M. Ylilammi, O. M. E. Ylivaara and R. L. Puurunen, Modeling growth kinetics of thin films made by atomic layer deposition in lateral high-aspect-ratio structures, *Journal of Applied Physics*, 2018, **123**, 205301.

[4] J. Yim, E. Verkama, J. A. Velasco, K. Arts and R. L. Puurunen, Conformality of atomic layer deposition in microchannels: impact of process parameters on the simulated thickness profile, *Physical Chemistry Chemical Physics*, 2022, **24**, 8645–8660.

[5] C. Gonsalves, J. A. Velasco, J. Yim, J. Järvilehto, V. Vuorinen and R. L. Puurunen, Simulated conformality of atomic layer deposition in lateral channels: the impact of the Knudsen number on the saturation profile characteristics, *Physical Chemistry Chemical Physics*, 2024, **26**, 28431–28448.

[6] J. Dendooven, *Atomically-Precise Methods for Synthesis of Solid Catalysts*, Royal Society of Chemistry, Cambridge, UK, 2014, vol. 22.

[7] C. Detavernier, J. Dendooven, S. P. Sree, K. F. Ludwig and J. A. Martens, Tailoring nanoporous materials by atomic layer deposition, *Chemical Society Reviews*, 2011, **40**, 5242–5253.

[8] E. W. Thiele, Relation between catalytic activity and size of particle, *Industrial & Engineering Chemistry*, 1939, **31**, 916–920.

[9] G. Bergeret and P. Gallezot, in *Handbook of Heterogeneous Catalysis*, Wiley-VCH, Weinheim, 2nd edn., 2008, vol. 2, ch. 3.1.2, pp. 738–765.

[10] Micromeritics Instrument Corporation, *AutoChem III Software*, 2025, Version 1.03 (593cf7a).

[11] J. Järvilehto, *Master's thesis*, Aalto University, 2023.

[12] F. Grillo, H. Van Bui, D. La Zara, A. A. Aarnink, A. Y. Kovalgin, P. Kooyman, M. T. Kreutzer and J. R. van Ommen, From single atoms to nanoparticles: Autocatalysis and metal aggregation in atomic layer deposition of Pt on TiO2 nanopowder, *Small*, 2018, **14**, 1800765.

[13] R. L. Puurunen, Surface chemistry of atomic layer deposition: A case study for the trimethylaluminum/water process, *Journal of Applied Physics*, 2005, **97**, 121301.

[14] J. Yim, E. Haimi, M. Mäntymäki, V. Kärkäs, R. Bes, A. A. Gutierrez, K. Meinander, P. Brüner, T. Grehl, L. Gell, T. Viinikainen, K. Honkala, S. Huotari, R. Karinen, M. Putkonen and R. L. Puurunen, Atomic Layer Deposition of Zinc Oxide on Mesoporous Zirconia Using Zinc(II) Acetylacetonate and Air, *Chemistry of Materials*, 2023, **35**, 7915–7930.